JOURNAL OF PROPULSION AND POWER
Vol. 34, No. 5, September–October 2018

Direct Wave-Drive Thruster

Matthew S. Feldman* and Edgar Y. Choueiri†
Princeton University, Princeton, New Jersey 08544

DOI: 10.2514/1.B36661

A propulsion concept relying on the direct steady-state acceleration of a plasma by an inductive wave-launching antenna is presented. By operating inductively in steady state, a direct wave-drive thruster (DWDT) avoids drawbacks associated with pulsed acceleration and electrode erosion. The generalized relations for the scaling of thrust and efficiency are derived analytically. Thrust is shown to scale with the square of the antenna current, and efficiency is shown to increase with increasing current or power. The total force and resistive losses between an annular antenna and a finite-conductivity plasma slab are modeled. Calculations from the model suggest four design criteria for efficient performance of a DWDT: the size of the device must be large when compared to both the standoff distance and plasma skin depth, the excitation frequency must be as large as the electron collision frequency, and the resistive losses within the wave-launching antenna must be minimized. A sample evaluation is performed with the model to illustrate the potential performance for a thruster operating at 10 kW with a mass flow rate of 1 mg/s at typical plasma parameters, and the maximum efficiency is found to have an upper bound near 50%.

Nomenclature

A, B, E	=	vector potential, magnetic field, and electric field
a	=	separation constant
C_T	=	thrust coefficient
D	=	dissipation parameter
J_a	=	current in wave-launching antenna
l	=	antenna–plasma standoff distance
$\dot{m}$	=	mass flow
P	=	power
$\overline{\overline{P}}_{\mathrm{EM}}$	=	Maxwell stress tensor
R	=	resistance
r, z	=	cylindrical coordinates
r_0	=	antenna size
T	=	thrust
v	=	velocity
α, γ	=	coupling parameters
δ_s	=	plasma skin depth
ϵ_0, μ_0, Z_0	=	permittivity, permeability, and impedance of free space
η	=	thrust efficiency
ν_e	=	electron collision frequency
σ	=	complex plasma conductivity
ω	=	antenna excitation angular frequency

I. Introduction

THE direct wave-drive thruster (DWDT) is a new steady-state propulsion concept that uses waves to transfer momentum directly to a plasma. By using an inductive wave-launching antenna (WLA), a DWDT can operate without electrodes, which prevents lifetime limitations associated with erosion processes seen in major propulsion concepts [1,2] and allows compatibility with a variety of propellants.

Most electrodeless accelerators can broadly be grouped into two categories: magnetic nozzles [3–5] and pulsed inductive accelerators [6–9], both of which suffer from various drawbacks. Magnetic nozzles often require a separate heating stage [3] and must address detachment concerns to avoid divergence losses [10,11]. Moreover, these devices are typically inefficient at low powers [4,5]. Meanwhile, high-power pulsed circuitry can degrade to limit thruster lifetime, and pulsed devices face technical challenges in limiting mass utilization losses [12]. By operating continuously and without a nozzle, a DWDT can potentially avoid these drawbacks. Some continuous devices using rotating electric fields have been explored [13,14], and another concept uses the ponderomotive force from electron cyclotron waves to directly accelerate electrons [15]. However, all of these devices may still rely on the expanding magnetic nozzle geometry for acceleration.

More recently, Jorns and Choueiri [16] proposed a direct wave-drive device that relied on the ponderomotive force obtained from damping beating electrostatic waves [17] to naturally generate thrust across magnetic field lines, and therefore did not rely on a magnetic nozzle topology. This force has already been explored to create plasma flows [18,19] and current drives [20,21] in fusion devices. However, theoretical investigations of these wave-driven flows have focused solely on the wave–plasma interaction within the plasma control volume. In the proposed concept, Jorns and Choueiri [16] did not consider the wave-launching mechanism and assumed waves were generated from an annular spiral antenna with no losses. Although this approach could describe momentum absorption, it ignored the inductive interactions that initially coupled momentum into the plasma from an antenna structure. For any direct wave-drive device, all of the momentum contained in the excited waves (and subsequently the bulk plasma) must be obtained from this inductive coupling. By analyzing this coupling, we can derive the general scaling behavior for both thrust and thrust efficiency.

The goals of this work are to present the DWDT concept, understand the fundamental physics governing the efficacy of the antenna–plasma interaction, and derive general and specific equations for the scaling of thrust and thrust efficiency. We start in Sec. II by describing the antenna–plasma momentum coupling for a general DWDT and deriving the scaling of thrust and thrust efficiency with increasing driving current. In Sec. III, we set up a simple annular DWDT configuration in order to calculate specific thrust and loss coefficients, and we use those coefficients to evaluate the scaling of thrust and efficiency as a function of various nondimensional parameters in Sec. IV. In Sec. V, we discuss the limitations of our assumptions and analytical approach as well as future design considerations; in Sec. VI, we summarize our findings.

II. Thrust and Efficiency Model

In its simplest form, the DWDT consists of a wave-launching antenna targeting the specific modes of a nearby plasma, as shown in Fig. 1.

Presented as Paper 2014-4025 at the 50th AIAA/ASME/SAE/ASEE Joint Propulsion Conference, AIAA Propulsion and Energy Forum, Cleveland, OH, 28–30 July 2014; received 26 February 2017; revision received 15 January 2018; accepted for publication 17 February 2018; published online 13 June 2018.

*Ph.D. Candidate, Electric Propulsion and Plasma Dynamics Laboratory, Mechanical and Aerospace Engineering Department. Student Member AIAA.

†Chief Scientist, Electric Propulsion and Plasma Dynamics Laboratory; Professor, Applied Physics Group. Fellow AIAA.

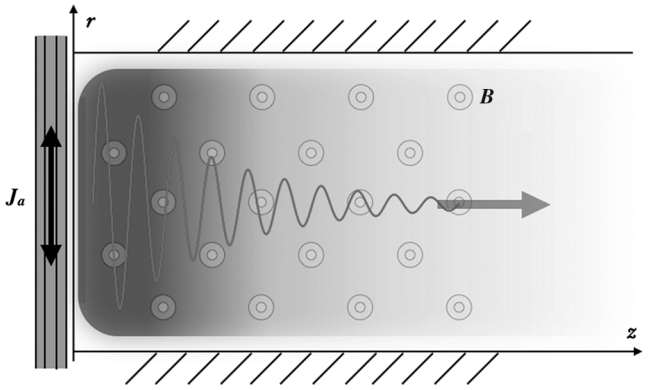

Fig. 1 Simple direct wave-drive thruster channel with an embedded magnetic field. A wave-launching antenna is placed behind the channel, which generates a propagating mode in the positive $\hat{z}$ direction.

The thruster may include an applied magnetic field that confines plasma away from the walls and can be tuned to create wave modes of interest inside of the thruster. And the wave-launching antenna may be used to couple to both propagating or nonpropagating wave modes.

Before delving into detailed analyses of the plasma wave modes or thruster geometry, it is useful to have a simplified analytical model that can predict the basic scaling behavior of thrust and efficiency for a wide range of DWDT parameters. To do this, we must first understand the basic thrust mechanisms and power loss mechanisms that will be dominant in such a concept. The major thrust contribution for a DWDT comes from momentum imparted to the plasma via the WLA. In our simplified model, we will neglect any cold gas and electrothermal thrust components. As a result, the total thrust can be calculated from the electromagnetic interaction between the plasma and the WLA. This force is applied continuously, so the total thrust is determined by time averaging these electromagnetic forces.

We approximate thrust efficiency by considering only the resistive and radiative losses associated with the antenna–plasma coupling. This ignores nonidealized effects, such as wall losses, frozen flow losses, and imperfect mass utilization. As a result, we derive an upper bound on the thrust efficiency constrained by the ohmic losses in the plasma and antenna, as well as the radiative energy losses from wave modes that do not contribute to thrust.

A. Thrust

The WLA is responsible for all momentum transferred to the plasma and acquired by the exhaust. As a result, we can calculate the total thrust by time averaging the electromagnetic pressure exerted on the plasma. Assuming little momentum is lost by radiation to vacuum, this total force exactly equals the force on the WLA. This assumption can be made when the excitation frequency is smaller than the plasma frequency because the plasma near the antenna surface reflects the vacuum mode so as to mostly cancel modes radiated in the opposite direction. As a result, the electromagnetic pressure between the WLA and plasma acts to both push the plasma and transfer thrust back to the antenna.

Therefore, the total electromagnetic thrust is simply the following:

$$T = \int_S \langle \overline{\overline{P}}_{\mathrm{EM}_{ij}} \rangle \cdot \mathrm{d}A \tag{1}$$

where the integral is taken over the surface of the plasma, which is similar to the derivations for self-field magnetoplasmadynamic thrusters (MPDTs) [22–24]. This electromagnetic pressure $\overline{\overline{P}}_{\mathrm{EM}_{ij}}$ is the typical Maxwell stress tensor

$$\overline{\overline{P}}_{\mathrm{EM}_{ij}} = \epsilon_0 \left(E_i E_j - \frac{1}{2}\delta_{ij} E^2 \right) + \frac{1}{\mu_0}\left(B_i B_j - \frac{1}{2}\delta_{ij} B^2 \right) \tag{2}$$

If we assume a linear response of the plasma to the excitation in the WLA, the magnitudes of the oscillating electric and magnetic fields are proportional to the magnitude of the exciting current in the WLA J_a. Therefore, the total pressure and total thrust must be proportional to the current squared:

$$T = C_T J_a^2 \tag{3}$$

and the thrust coefficient C_T is dependent on the geometry of the system, the excitation frequency, and the plasma response. We present an explicit calculation of C_T in an annular DWDT configuration in Sec. III.

B. Efficiency

We can determine the scaling of thrust efficiency by determining the total thrust power and the power dissipated by the various loss mechanisms. Thrust power is dependent on mass flow and is given by

$$P_T = \frac{T^2}{2\dot{m}} \tag{4}$$

The dominant loss mechanisms are resistive and radiative in nature. In the plasma, ohmic heating can be calculated with

$$P_{L,\mathrm{plasma}} = \int \langle \boldsymbol{J}_p \cdot \boldsymbol{E} \rangle \, \mathrm{d}V \tag{5}$$

where $\boldsymbol{J}_p$ and $\boldsymbol{E}$ are the currents and electric fields in the plasma, and we integrate over the full plasma volume. Again, assuming a linear response, both terms are proportional to the excitation current in the WLA J_a. The resistive and radiative losses from the WLA are simply

$$P_{L,\mathrm{wla}} = \langle R_{\mathrm{wla}} J_a^2 \rangle, \qquad P_{L,\mathrm{rad}} = \langle R_{\mathrm{rad}} J_a^2 \rangle \tag{6}$$

Putting these losses together, the total power loss is

$$P_L = \langle (R_{\mathrm{plasma}} + R_{\mathrm{wla}} + R_{\mathrm{rad}}) J_a^2 \rangle = \frac{1}{2} R_{\mathrm{eff}} J_a^2 \tag{7}$$

where R_{eff} is the overall effective resistance of the combined losses, and the factor of $1/2$ comes from time averaging over the oscillation.

Finally, the efficiency of the thrust transfer is thrust power divided by total power. That is,

$$\eta = \frac{P_T}{P_T + P_L} = \frac{1}{1 + (\dot{m} R_{\mathrm{eff}} / C_T^2 J_a^2)} \tag{8}$$

where R_{eff} is a loss coefficient that can have, like C_T, a complicated dependence on geometry and plasma dynamics. Although thrust in a DWDT scales with the current squared, thrust efficiency also improves with increasing current. This scaling behavior is quite similar to that derived for self-field MPDTs [24], except that the generated electromagnetic pressure is coupled to the plasma inductively.

III. Thrust and Loss Coefficient Derivations

The basic scaling behavior of a DWDT with respect to the antenna current is straightforward. When assuming a linear response, an efficient thruster can be created with sufficient current or power. However, in order to determine how much power is required to create an efficient device, we must understand how both C_T and R_{eff} are affected by the configuration of the WLA, the properties of the plasma, and the targeted wave modes. In this section, we will calculate the thrust and efficiency for a specific configuration in order to bound thruster performance. To do this, we will not consider a propagating mode but, instead, an evanescing, ordinary wave, which simplifies the analysis while retaining the salient scaling features. However, this assumption ignores the difficulty that may arise in accessing other wave modes.

We start by taking the antenna to have a fixed annular geometry similar to the antenna configurations used in pulsed inductive thrusters (PITs) [6,7] and proposed for devices like the ponderomotive thruster [16]. We assume the current is distributed evenly through a flat annulus with the inner radius r_0 and outer radius $2r_0$ positioned

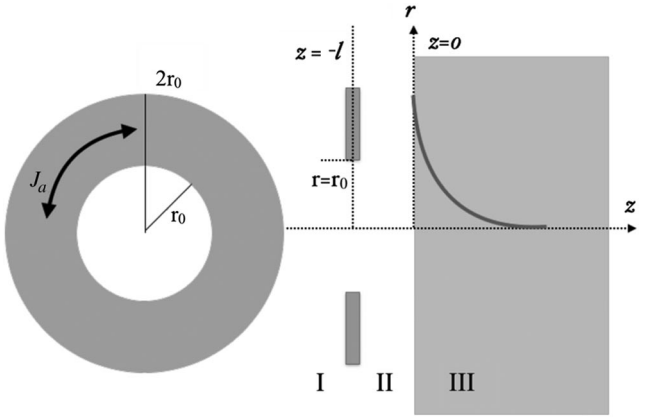

Fig. 2 Solution geometry for a fixed annular antenna. Evanescing wave mode shown in region III.

parallel to a flat plasma surface at a standoff distance l as shown in Fig. 2. We further simplify the model by treating the plasma as a uniform semi-infinite slab occupying a half-space a fixed distance from the annular WLA and assume the plasma is preionized in order to isolate the antenna–plasma interaction. Finally, we do not include a background magnetic field. As a result, only the collisional, evanescing ordinary mode is present in the plasma. And, we note that the approximation of a plasma with infinite extent holds well for high plasma conductivities, which will correspond to stronger coupling between the WLA and the plasma.

To calculate the thrust coefficient C_T and the plasma resistance R_{plasma}, we assume an oscillating source current with magnitude J_a in the WLA and solve Maxwell's equations throughout the geometry. Once we have solved for the electric and magnetic fields, the force on the plasma can be immediately determined. The currents and fields in the plasma are determined by the frequency-dependent plasma conductivity, which is primarily a function of the plasma density, and the electron collision frequency.

A. Magnetic Vector Potential Solution

In this configuration, it is easiest to calculate the electric and magnetic fields via the magnetic vector potential $\boldsymbol{A}$, where

$$\boldsymbol{B} = \nabla \times \boldsymbol{A}, \qquad \boldsymbol{E} = -\frac{\partial \boldsymbol{A}}{\partial t}, \qquad \boldsymbol{J} = -\sigma \frac{\partial \boldsymbol{A}}{\partial t} \tag{9}$$

Because of the cylindrical symmetry, $\boldsymbol{A}$ is purely the azimuthal direction, and the wave equation becomes

$$\nabla^2 \boldsymbol{A} - \frac{1}{c^2}\frac{\partial^2 \boldsymbol{A}}{\partial t^2} - \mu_0 \sigma \frac{\partial \boldsymbol{A}}{\partial t} = \mu_0 \boldsymbol{J_0} \tag{10}$$

where σ is the frequency-dependent conductivity, which is zero in free space; and $\boldsymbol{J}_0 = (J_a/r_0)\delta(z+l)$ is the excitation current density in the WLA. To solve, we allow J_a and $\boldsymbol{A}$ to vary sinusoidally with a given frequency, such that $\boldsymbol{A} = \boldsymbol{A}_s e^{i\omega t}$, where $\boldsymbol{A}_s$ is the spatially varying part of $\boldsymbol{A}$ and is complex valued. The complex conductivity can be obtained from the electron momentum equation:

$$\sigma = \frac{e^2 n_e}{m_e(\nu_e + i\omega)} = \frac{1}{\mu_0}\frac{\omega_{pe}^2}{c^2}\frac{1}{\nu_e + i\omega} \tag{11}$$

where m_e is the mass of an electron, n_e is the electron density, and ν_e is the electron collision frequency.

Finally, we assume that the input frequencies are sufficiently small that the second-order time derivative is negligible. This assumption is justified when $\omega, \nu \ll \omega_{pe}$: the latter of which is true for typical plasma parameters relevant to electric propulsion devices. And, we have

$$\nabla^2 \boldsymbol{A}_s - \frac{\omega_{pe}^2}{c^2}\frac{i\omega}{\nu_e + i\omega}\boldsymbol{A}_s = \mu_0 \boldsymbol{J_0} \tag{12}$$

We solve for $\boldsymbol{A}$ by closely following the solution used by Dodd and Deeds [25], who solved a similar configuration using a single coil near a material with purely real conductivity. However, we use Eq. (11) and integrate over many loops to form a flat annular antenna. Like in other wave-coupling solutions [26], we split the solution space into separate domains (shown in Fig. 2) corresponding to $z < -l$, $-l < z < 0$, and $z > 0$; we solve each domain separately; and then we match boundary conditions in order to stitch together a unique self-consistent solution. Before proceeding, we nondimensionalize Eq. (12) using the following scheme based on the geometry described previously:

$$\bar{r} = r/r_0 \qquad \bar{z} = z/r_0 \qquad \bar{l} = l/r_0 \qquad \delta_s = c/\omega_{pe}$$
$$\bar{\delta}_s = \delta_s/r_0 \qquad \bar{\nu} = \nu_e/\omega \qquad \tau = \omega t$$

where $\bar{r}$ and $\bar{z}$ are the normalized cylindrical coordinates, l is the antenna–plasma standoff distance, and δ_s is the classical plasma skin depth.

In regions I and II, there is no plasma; and the vector potential diffusion equation becomes

$$\nabla^2 \boldsymbol{A}_s = 0 \tag{13}$$

where ∇ is now the spatial gradient with respect to the normalized coordinate system. In region III, the equation becomes

$$\nabla^2 \boldsymbol{A}_s - \bar{\delta}_s^{-2}\frac{1}{\sqrt{1+\bar{\nu}^2}} e^{i\tan^{-1}\bar{\nu}} \boldsymbol{A}_s = 0 \tag{14}$$

Finally, we define $\theta_\nu = \tan^{-1}\bar{\nu}$, where θ_ν is between zero and $\pi/2$, so that

$$\nabla^2 \boldsymbol{A}_s - \bar{\delta}_s^{-2}\cos\theta_\nu e^{i\theta_\nu} \boldsymbol{A}_s = 0 \tag{15}$$

This is expanded into the cylindrical coordinate system:

$$\frac{1}{\bar{r}}\frac{\partial}{\partial \bar{r}}\left(\bar{r}\frac{\partial \boldsymbol{A}_s}{\partial \bar{r}}\right) - \frac{\boldsymbol{A}_s}{\bar{r}^2} + \frac{\partial^2 \boldsymbol{A}_s}{\partial \bar{z}^2} - \bar{\delta}_s^{-2}\cos\theta_\nu e^{i\theta_\nu}\boldsymbol{A}_s = 0 \tag{16}$$

To calculate the forces on and dissipation within the plasma, we only need to know $\boldsymbol{A}$ in region III, but we need to solve for the equations in all three regions simultaneously. The full derivation is performed in the Appendix and yields

$$\boldsymbol{A}_{3s} = \mu_0 J_a \int_0^\infty \int_1^2 x J_1(ax) J_1(a\bar{r}) \times \frac{a}{a + \sqrt{a^2 + \bar{\delta}_s^{-2}\cos\theta_\nu e^{i\theta_\nu}}} e^{-a\bar{l}} e^{-\sqrt{a^2+\bar{\delta}_s^{-2}\cos\theta_\nu e^{i\theta_\nu}}\bar{z}}\,\mathrm{d}x\,\mathrm{d}a \tag{17}$$

where J_1 is a Bessel function of the first kind; and we are integrating over a, the spatial separation constant, and x the normalized surface of the annulus. The time-dependent solution is further normalized by defining $\bar{\boldsymbol{A}} = \boldsymbol{A}/(\mu_0 J_a)$ such that

$$\bar{\boldsymbol{A}}(\bar{r},\bar{z},\bar{k}_s,\bar{l},\theta_\nu,\tau) = e^{i\tau}\int_0^\infty \int_1^2 x J_1(ax) J_1(a\bar{r}) \times \frac{a}{a + \sqrt{a^2 + \bar{\delta}_s^{-2}\cos\theta_\nu e^{i\theta_\nu}}} e^{-a\bar{l}} e^{-\sqrt{a^2+\bar{\delta}_s^{-2}\cos\theta_\nu e^{i\theta_\nu}}\bar{z}}\,\mathrm{d}x\,\mathrm{d}a \tag{18}$$

B. Thrust Coefficient C_T

The net electromagnetic force generated on the plasma can be calculated from the integration of the $\boldsymbol{J}\times\boldsymbol{B}$ force density in the plasma:

$$\boldsymbol{F} = \int Re[\boldsymbol{J}] \times Re[\boldsymbol{B}]\,\mathrm{d}V \tag{19}$$

Using Eq. (9) and the normalization scheme,

$$\boldsymbol{F} = \mu_0 J_a^2 \int Re[-\bar{\delta}_s^{-2}\cos\theta_\nu e^{i\theta_\nu}\bar{\boldsymbol{A}}] \times Re[\nabla \times \bar{\boldsymbol{A}}]\,\mathrm{d}\bar{V} \tag{20}$$

Because $\boldsymbol{A}$ is only in the $\hat{\theta}$ direction, we can rewrite the force into the component in the $\hat{z}$ (i.e., thrust) direction as

$$F_z = -\mu_0 J_a^2 \bar{\delta}_s^{-2}\cos\theta_\nu \int Re[e^{i\theta_\nu}\bar{\boldsymbol{A}}] \cdot Re\left[\frac{\partial \bar{\boldsymbol{A}}}{\partial \bar{z}}\right]\mathrm{d}\bar{V} \tag{21}$$

By time averaging the total axial force and applying the divergence theorem, we get

$$T = \frac{\pi}{2}\mu_0 J_a^2 \bar{\delta}_s^{-2}\cos^2\theta_\nu \int_0^\infty \|\bar{\boldsymbol{A}}_s(\bar{r}, \bar{z}=0, \bar{\delta}_s, \bar{l}, \theta_\nu)\|^2 \bar{r}\,\mathrm{d}\bar{r} \tag{22}$$

The maximum force ($T_{\max} = (3/4)\pi\mu_0 J_a^2$) occurs as $\bar{\delta}_s, \bar{l}, \theta_\nu \to 0$. Physically, this occurs when the plasma density is sufficiently high and the electron collision frequency and standoff distance are sufficiently small. This result is not surprising because $T_{\max}$ is equal to the magnetic pressure between two infinite current sheets [27] multiplied by the area of the antenna and an additional factor of $1/2$ to account for the average over the period of oscillation.

Normalizing by this maximum force, we get

$$T(\bar{\delta}_s, \bar{l}, \theta_\nu, J_a) = T_{\max} \cdot \gamma(\bar{\delta}_s, \bar{l}, \theta_\nu) \tag{23}$$

where

$$\gamma(\bar{\delta}_s, \bar{l}, \theta_\nu) = \int_0^\infty \frac{2}{3}\bar{r}\left\| \int_0^\infty \int_1^2 xJ_1(ax)J_1(a\bar{r}) \times \frac{a\bar{\delta}_s^{-1}\cos\theta_\nu}{a + \sqrt{a^2 + \bar{\delta}_s^{-2}\cos\theta_\nu e^{i\theta_\nu}}} e^{-a\bar{l}}\,\mathrm{d}x\,\mathrm{d}a \right\|^2 \mathrm{d}\bar{r} \tag{24}$$

and is between zero and one.

Therefore, the thrust coefficient C_T is given by the following:

$$C_T = \frac{3}{4}\pi\mu_0\gamma(\bar{\delta}_s, \bar{l}, \theta_\nu) \tag{25}$$

C. Plasma Resistance R_{plasma}

The power dissipation in the plasma is calculated from the integration of joule heating in the plasma:

$$P_{L,\text{plasma}} = \int \langle Re[\boldsymbol{J}] \cdot Re[\boldsymbol{E}]\rangle\,\mathrm{d}V \tag{26}$$

Again, using Eq. (9) and the normalization scheme, we have

$$P_{L,\text{plasma}} = \left\langle Z_0 J_a^2 \bar{\delta}_s^{-3}\frac{\omega}{\omega_{pe}}\cos\theta_\nu \int_0^\infty \int_0^\infty \{Re[e^{i\theta_\nu}\bar{\boldsymbol{A}}] \cdot Re[i\bar{\boldsymbol{A}}]\}\bar{r}\,\mathrm{d}\bar{r}\,\mathrm{d}\bar{z}\right\rangle \tag{27}$$

And, the time-averaged result is

$$P_{L,\text{plasma}} = \pi Z_0 J_a^2 \bar{\delta}_s^{-3}\frac{\nu_e}{\omega_{pe}}\cos^2\theta_\nu \int_0^\infty \int_0^\infty \|\bar{\boldsymbol{A}}_s(\bar{r}, \bar{z}, \bar{\delta}, \bar{l}, \theta_\nu)\|^2 \bar{r}\,\mathrm{d}\bar{r}\,\mathrm{d}\bar{z} = \frac{1}{2}R_{\text{plasma}} J_a^2 \tag{28}$$

We can normalize the plasma resistance in a similar manner to C_T by separating a new coupling parameter α from a term dependent on the ratio of ν_e to ω_{pe}:

$$R_{\text{plasma}} = \frac{3}{2}\pi Z_0 J_a^2 \frac{\nu_e}{\omega_{pe}} \cdot \alpha(\bar{\delta}_s, \bar{l}, \theta_\nu) \tag{29}$$

where

$$\alpha(\bar{\delta}_s, \bar{l}, \theta_\nu) = \bar{\delta}_s^{-1}\int_0^\infty \int_0^\infty \frac{4}{3}\bar{r}\left\| \int_0^\infty \int_1^2 xJ_1(ax)J_1(a\bar{r}) \times \frac{a\bar{\delta}_s^{-1}\cos\theta_\nu}{a + \sqrt{a^2 + \bar{\delta}_s^{-2}\cos\theta_\nu e^{i\theta_\nu}}} e^{-a\bar{l}} e^{-\sqrt{a^2+\bar{\delta}_s^{-2}\cos\theta_\nu e^{i\theta_\nu}}\,\bar{z}}\,\mathrm{d}x\,\mathrm{d}a \right\|^2 \mathrm{d}\bar{r}\,\mathrm{d}\bar{z} \tag{30}$$

and is also between zero and one.

IV. Parametric Investigation of Thrust and Thrust Efficiency

A. Scaling of the Thrust Coefficient and Plasma Resistance with Nondimensional Quantities

We now have analytical descriptions for C_T and R_{plasma} as functions of three nondimensional parameters $\bar{\delta}_s$, $\bar{l}$, and $\bar{\nu}$. The interplay of these three parameters is seen in Eqs. (24) and (30) for γ and α: both of which go to unity as $\bar{\delta}_s, \bar{l}, \bar{\nu} \to 0$. These equations do not have explicit solutions in terms of elementary functions; therefore, we performed numerical integrations over a parameter space from $\bar{\delta}_s = 1$ to $1/64$, $\bar{l} = 1$ to $1/16$, and $\bar{\nu} = 1/10$ to 10 ($\theta_\nu = .1$ to 1.47).

Figure 3 shows contour plots for the coupling parameter γ in terms of $\bar{\delta}_s$ and $\bar{l}$ for various values of $\bar{\nu}$. As expected, we can see that γ increases toward unity as $\bar{\delta}_s, \bar{l}, \bar{\nu} \to 0$. In the reverse direction, γ quickly decreases to zero. The parameters α and γ exhibit similar behavior so that, as γ increases, the dissipation losses also increase. Qualitatively, this occurs because more current must be present in the plasma in order to increase the net force. This additional current leads to more ohmic heating.

B. Efficiency

By recalling Eq. (8) and ignoring losses from R_{wla} and R_{rad}, we have

$$\eta = \frac{1}{1 + (\dot{m}R_{\text{plasma}}/C_T^2 J_a^2)} = \frac{1}{1 + D_P} \tag{31}$$

where

$$D_P = \frac{\dot{m}R_{\text{plasma}}}{C_T^2 J_a^2} \tag{32}$$

is a normalized dissipation parameter. Substituting Eqs. (25) and (29) gives us

$$D_P = \frac{8\dot{m}c}{3\pi\mu_0 J_a^2}\frac{\nu_e}{\omega_{pe}}\frac{\alpha}{\gamma^2} \tag{33}$$

where efficiency is improved by minimizing D_P. This can be achieved by increasing the total current in the antenna, and therefore the total power of the device, or by minimizing the ratio of α/γ^2, the ratio of ν_e/ω_{pe}, or the mass flow rate.

We put the aforementioned model in perspective by making assumptions typical of an electric propulsion device; $\dot{m} = 1$ mg/s, $r_0 = 4$ cm, $l = 1$ cm, $n_e = 3 \times 10^{17}$ m^{-3}, and $T_e = 5$ eV, such that $\bar{\delta}_s = 1/4$ and $\bar{l} = 1/4$. For these values, the thrust efficiency can be calculated by assuming various $\bar{\nu}$. Figure 4 shows plots of efficiency as a function of power for a range of $\bar{\nu}$. Clearly, improved performance occurs for smaller electron collision frequencies or higher input frequencies, which is the parameter most easily experimentally controlled.

We can account for resistive losses in the WLA by deriving a second dissipation parameter:

$$D_{\text{wla}} = \frac{16\dot{m}R_{\text{wla}}}{9\pi^2\mu_0^2 J_a^2}\frac{1}{\gamma^2} \tag{34}$$

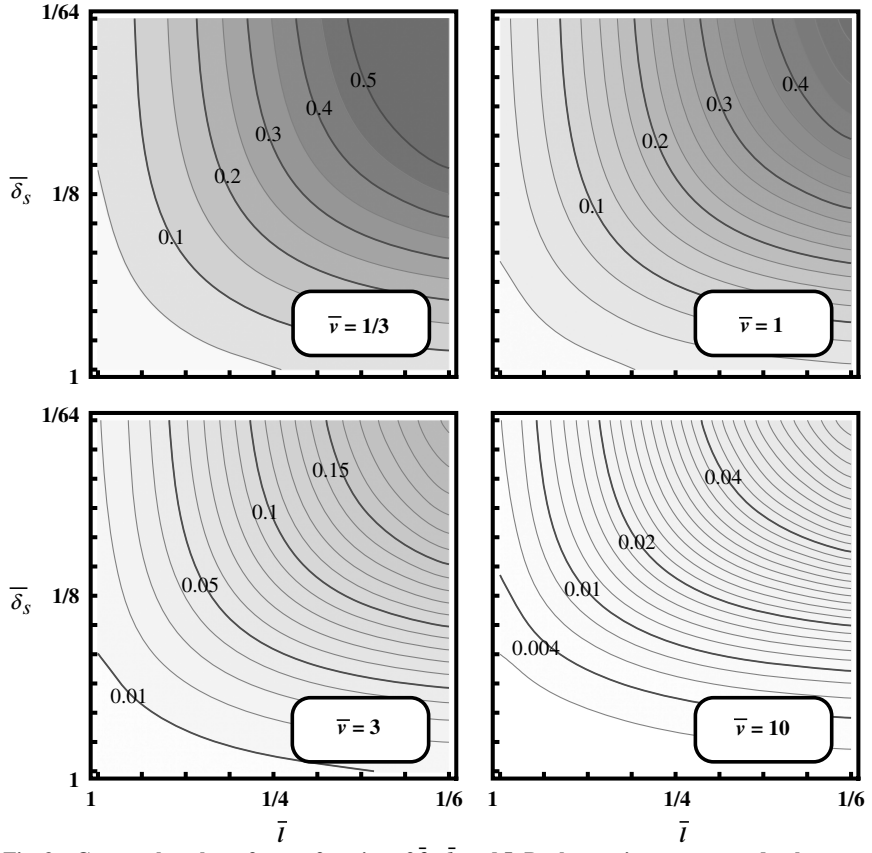

Fig. 3 Contour log plots of γ as a function of $\bar{\delta}_s$, $\bar{l}$, and $\bar{\nu}$. Darker regions correspond to larger γ.

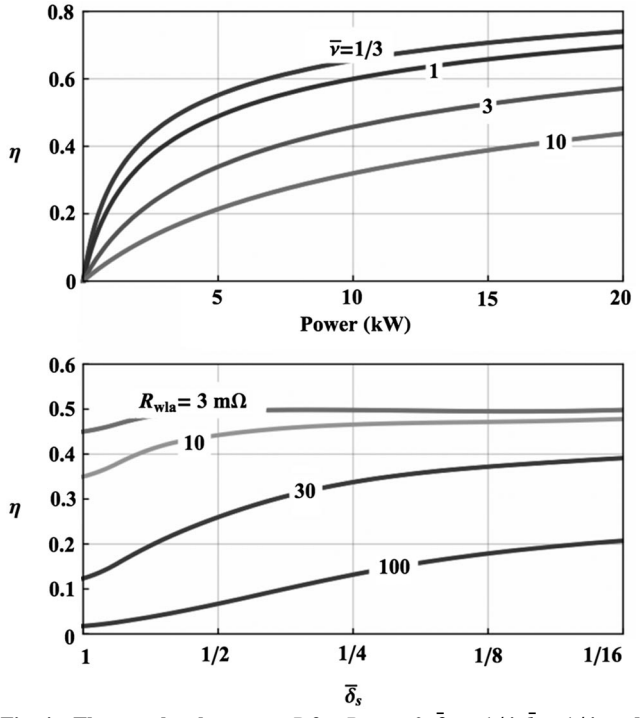

Fig. 4 The top plot shows η vs P for $R_{\text{wla}} = 0$, $\bar{\delta}_s = 1/4$, $\bar{l} = 1/4$, and increasing $\bar{\nu}$. The bottom plot shows η vs $\bar{\delta}_s$ for $P = 5$ kW, $\bar{\nu} = 1/3$, $\bar{l} = 1/4$, and increasing R_{wla}.

which is the ratio of power dissipated in the WLA to the thrust power. In Fig. 4, we hold the total input power fixed at 5 kW and vary the WLA resistance R_{wla} while plotting efficiency against the nondimensional skin depth $\bar{\delta}_s$. We find that decreasing both the skin depth and resistance improves the calculated efficiency.

This efficiency calculation ignores other system losses, such as the ionization energy required to create the plasma. At lower powers, we expect this may significantly reduce overall performance. We can estimate the power requirement by assuming the plasma plume is fully ionized and that none of the ionization energy is recovered. For singly ionized xenon, assuming $\dot{m} = 1$ mg/s and noting that the first ionization energy is $E_i \approx 12$ eV, this corresponds to ~10 W. Even for particularly inefficient ionization and maintenance schemes, the overall losses are comparably small for a device operating with greater than 1 kW.

C. Thruster Design Considerations

We have analytically modeled a simplified DWDT concept and shown that, in addition to J_a, the scaling of thrust and thrust efficiency depends on three important nondimensional parameters: $\bar{\nu}$, $\bar{l}$, and $\bar{\delta}_s$. Although the most straightforward method for improving efficiency is to increase the total power, coupling and efficiency can be improved as $\bar{\nu}$, $\bar{l}$, and $\bar{\delta}_s \to 0$. Practically speaking, δ_s and l are difficult to decrease because $\delta_s \sim n_e^{-1/2}$ and l is dependent on the amount of material insulating the WLA. Therefore, $\bar{l}$ and $\bar{\delta}_s$ are most easily controlled by increasing the physical size of the thruster r_0. Meanwhile, $\bar{\nu}$ can be easily minimized by increasing the applied frequency ω.

V. Discussion

The preceding analysis uses a number of simplifying assumptions that may affect the performance of a practical device. First, by assuming an infinite-extent plasma, we have artificially limited fringe effects. Second, by assuming a constant density plasma, we have ignored the wave-absorption dynamics that are likely to occur for various wave modes. Additionally, we have ignored ionization costs in our efficiency calculation, which would further reduce the

expected performance. Finally, by choosing a linear, ordinary coupling to the plasma, we have ignored potential optimizations that might exist by targeting specific wave modes.

The linearity assumption also limits the application of our theory because increasing power levels will eventually reach nonlinear regimes. At such power levels, a DWDT behavior may change to the extent that it is quite similar to a PIT operated continuously, where significant density rarefactions limit the antenna–plasma coupling. However, the instantaneous power levels delivered in pulsed concepts can exceed 1 MW [6,7], which is far beyond what could reasonably be delivered continuously. It is useful to see what power levels may cause less extreme nonlinear effects. For example, the power level where the linearity assumption might first break down can be determined by comparing the distance traveled by an electron during an oscillation to the overall size of the device: $r_0 > L \sim v/\omega$. Using Eq. (9) and the electron equation of motion, we get that $L \sim eA/m_e\omega < r_0$. For a 10 MHz driving frequency, and the typical parameters previously used, the inequality breaks down near 10 kW of thrust power, which is comparable to powers used for current electric propulsion concepts.

This power level is also near where we begin to see reasonable efficiencies from our analysis in Sec. IV. One way to potentially overcome this limitation is through an applied magnetic field that favorably alters the coupling behavior between the WLA and plasma. For example, Alfvén waves can be accessed by the addition of a background magnetic field, and they are capable of carrying significant momentum. The linearity of such waves is dependent on the ratio of the wave magnetic field to the applied magnetic field so, by increasing the background field strength, linearity can be maintained at higher powers. The addition of an applied field may also influence the WLA–plasma coupling by altering the plasma skin depth and the associated dissipation losses. Finally, such a field also serves to confine the plasma near the WLA to help ensure stronger coupling.

VI. Conclusions

A new concept was presented for a plasma thruster that is electrodeless, nozzleless, and continuous while avoiding life-limiting effects from erosion and high-power pulsed circuitry without encountering the detachment concerns of a magnetic nozzle. Further described was the appropriate method of analyzing the thrust and thrust efficiency by solving the momentum and the energy coupling between the wave-launching antenna structure and the plasma.

From this approach, it is seen that a DWDT will have a thrust proportional to the WLA current squared J_a^2 and that efficiency of the momentum coupling will increase as the current and power are increased. By analyzing a specific configuration and calculating thrust and loss coefficients, four design criterion are determined for effective performance:

1) The size of the device should be larger than the plasma skin depth; $r_0 > \delta_s$.

2) The size of the WLA should be larger than the standoff distance; $r_0 > l$.

3) The excitation frequency should be larger the electron collision frequency; $\omega > \nu_e$.

4) The resistive losses within the WLA must be minimized; $R_{\text{wla}} \to 0$.

The aforementioned design constraints were derived for the coupling between the WLA and a linear, ordinary mode. Qualitatively, they could be understood as requiring the maximum momentum coupling from the WLA to the plasma while minimizing the associated dissipative losses. For typical laboratory plasma parameters analyzed in Sec. IV, it was shown that a DWDT would achieve reasonable efficiencies while remaining linear, with up to approximately 10 kW of power.

The analysis of the ordinary mode illuminates the limits of thrust scaling, particularly at powers below 10 kW. As nonlinearities become relevant, other modes may be of primary interest, such as Alfvén modes, which may be targeted with specific applied magnetic fields. A thruster based on these wave modes is expected to rely on similar design constraints that are dependent on each specific mode.

Appendix: Calculation of the Vector Potential

Starting with Eqs. (13) and (16), we apply separation of the variables on $\boldsymbol{A}_s$ such that

$$\boldsymbol{A}_s = R(\bar{r}) \cdot Z(\bar{z}) \tag{A1}$$

and define a separation constant a^2. Therefore, the solution can be described by

$$\frac{1}{\bar{r}R}\frac{\partial}{\partial \bar{r}}\left(\bar{r}\frac{\partial R}{\partial \bar{r}}\right) - \frac{1}{\bar{r}^2} = -a^2 \tag{A2}$$

$$\frac{1}{Z}\frac{\partial^2 Z}{\partial \bar{z}^2} = \begin{cases} a^2 & \text{Region I and II} \\ b^2 & \text{Region III} \end{cases} \tag{A3}$$

where $b^2 = a^2 + \bar{\delta}_s^{-2}\cos\theta_\nu e^{i\theta_\nu}$. The solutions to the R equation are Bessel functions of the first and second kinds. However, only Bessel functions of the first kind are physical. The Z equation has growing and decaying exponential solutions where, physically, region I can only have growing exponentials and region III can only have decaying exponentials.

As a result, the solutions to Eqs. (13) and (16) in each region are as follows:

$$\boldsymbol{A}_{1s}(\bar{r},\bar{z}) = \int_0^\infty [C_1(a)e^{a\bar{z}}J_1(a\bar{r})]\,\mathrm{d}a \tag{A4}$$

$$\boldsymbol{A}_{2s}(\bar{r},\bar{z}) = \int_0^\infty [(C_2(a)e^{a\bar{z}} + C_3(a)e^{-a\bar{z}})J_1(a\bar{r})]\,\mathrm{d}a \tag{A5}$$

$$\boldsymbol{A}_{3s}(\bar{r},\bar{z}) = \int_0^\infty [C_4(a)e^{-b\bar{z}}J_1(a\bar{r})]\,\mathrm{d}a \tag{A6}$$

And, C_i is the amplitude of each mode. Dodd and Deeds [25] previously generated and solved similar equations when the excitation term in Eq. (10) was a single coil loop and the material had multiple layers of purely real conductivities. We proceed using their methodology. However, instead of a single loop, we have an annular antenna, so we will use their solution and integrate over many loops to form a full annulus. Assuming a single coil loop with a radius x in normalized coordinates and a fixed current J_a, the appropriate boundary conditions are as follows:

$$\boldsymbol{A}_{1s}(\bar{r},-\bar{l}) = \boldsymbol{A}_{2s}(\bar{r},-\bar{l}) \tag{A7}$$

$$\boldsymbol{A}_{2s}(\bar{r},0) = \boldsymbol{A}_{3s}(\bar{r},0) \tag{A8}$$

$$\left.\frac{\partial \boldsymbol{A}_{1s}}{\partial \bar{z}}\right|_{\bar{z}=-\bar{l}} = \left.\frac{\partial \boldsymbol{A}_{2s}}{\partial \bar{z}}\right|_{\bar{z}=-\bar{l}} + \mu_0 J_a \delta(\bar{r}-x) \tag{A9}$$

$$\left.\frac{\partial \boldsymbol{A}_{2s}}{\partial \bar{z}}\right|_{\bar{z}=0} = \left.\frac{\partial \boldsymbol{A}_{3s}}{\partial \bar{z}}\right|_{\bar{z}=0} \tag{A10}$$

Solving these four equations for the unknown C_i, we have

$$C_1(a) = \frac{1}{2}\mu_0 J_a x J_1(ax)\left[\frac{a-b}{a+b}e^{-a\bar{l}} + e^{a\bar{l}}\right] \tag{A11}$$

$$C_2(a) = \frac{1}{2}\mu_0 J_a x J_1(ax)\frac{a-b}{a+b}e^{-a\bar{l}} \tag{A12}$$

$$C_3(a) = \frac{1}{2}\mu_0 J_a x J_1(ax) e^{-a\bar{l}} \tag{A13}$$

$$C_4(a) = \mu_0 J_a x J_1(ax) \frac{a}{a+b} e^{-a\bar{l}} \tag{A14}$$

To calculate the forces and losses in the plasma, we are solely concerned with region III, and the magnetic vector potential in that region is as follows:

$$\boldsymbol{A}_{3\text{loop}}(\bar{r},\bar{z}) = \mu_0 J_a \int_0^\infty \left[x J_1(ax) J_1(a\bar{r}) \frac{a}{a+b} e^{-a\bar{l}} e^{-b\bar{z}} \right] \mathrm{d}a \tag{A15}$$

A full annulus with an inner radius r_0 and an outer radius $2r_0$ can be thought of as many individual coils with radii between r_0 and $2r_0$, which correspond to $x = 1$ and $x = 2$ in the normalized coordinate system. Each individual coil has a fraction of the total antenna current J_a. Taking the limiting behavior as infinitely many coils with J_a evenly distributed among them, we get a total magnetic vector potential by integrating over x:

$$\boldsymbol{A}_{3s}(\bar{r},\bar{z}) = \mu_0 I_a \int_1^2 \int_0^\infty \left[x J_1(ax) J_1(a\bar{r}) \frac{a}{a+b} e^{-a\bar{l}} e^{-b\bar{z}} \right] \mathrm{d}a \; \mathrm{d}x \tag{A16}$$

Acknowledgment

This research was supported by the Program in Plasma Science and Technology at Princeton University.

References

[1] Goebel, D., and Katz, I., *Fundamentals of Electric Propulsion: Ion and Hall Thrusters*, Wiley, Hoboken, NJ, 2008, pp. 230–235, 306–309.

[2] Choueiri, E. Y., and Ziemer, J., "Quasi-Steady Magnetoplasmadynamic Thruster Performance Database," *Journal of Propulsion and Power*, Vol. 17, No. 5, 2001, pp. 967–976. doi:10.2514/2.5857

[3] Diaz, F., "The Vasimr Rocket," *Scientific American*, Vol. 283, No. 5, Nov. 2000, pp. 90–97. doi:10.1038/scientificamerican1100-90

[4] Takahashi, K., Charles, C., Boswell, R., and Ando, A., "Performance Improvement of a Permanent Magnet Helicon Thruster," *Journal of Physics D: Applied Physics*, Vol. 46, No. 35, 2013, Paper 352001. doi:10.1088/0022-3727/46/35/352001

[5] Jarrige, J., Elias, P., Cannat, F., and Packan, D., "Performance Comparison of an ECR Plasma Thruster Using Argon and Xenon as Propellant Gas," *33rd International Electric Propulsion Conference*, IEPC Paper IEPC-2013-420, Washington, D.C., Oct. 2013.

[6] Lovberg, R., and Dailey, C., "PIT Mark V Design," *Conference on Advanced SEI Technologies*, AIAA Paper 1991-3571, Sept. 1991. doi:10.2514/6.1991-3571

[7] Choueiri, E. Y., and Polzin, K., "Faraday Acceleration with Radio-Frequency Assisted Discharge," *Journal of Propulsion and Power*, Vol. 22, No. 3, 2006, pp. 611–619. doi:10.2514/1.16399

[8] Brown, D., Beal, B., and Haas, J., "Air Force Research Laboratory High Power Electric Propulsion Technology Development," *2010 IEEE Aerospace Conference*, IEEE Publ., Piscataway, NJ, March 2010, pp. 1–9. doi:10.1109/AERO.2010.5447035

[9] Slough, J., Kirtley, D., and Weber, T., "Pulsed Plasmoid Propulsion: The ELF Thruster," *31st International Electric Propulsion Conference*, IEPC Paper IEPC-2009-265, Ann Arbor, MI, Sept. 2009.

[10] Ahedo, E., and Merino, M., "On Plasma Detachment in Propulsive Magnetic Nozzles," *Physics of Plasmas*, Vol. 18, No. 5, 2011, Paper 053504. doi:10.1063/1.3589268

[11] Arefiev, A., and Breizman, B., "Magnetohydrodynamic Scenario of Plasma Detachment in a Magnetic Nozzle," *Physics of Plasmas*, Vol. 12, No. 4, 2005, Paper 043504. doi:10.1063/1.1875632

[12] Polzin, K., "Comprehensive Review of Planar Pulsed Inductive Plasma Thruster Research and Technology," *Journal of Propulsion and Power*, Vol. 27, No. 3, 2011, pp. 513–531. doi:10.2514/1.B34188

[13] Toki, K., Shinohara, S., Tanikawa, T., Hada, T., Funaki, I., Tanaka, Y., Yamaguchi, A., and Shamrai, K. P., "On the Electrodeless MPD Thruster Using a Compact Helicon Plasma Source," *44th AIAA/ASME/SAE/ASEE Joint Propulsion Conference*, AIAA Paper 2008-4729, July 2009. doi:10.2514/6.2008-4729

[14] Satoh, S., Matsuoka, T., Fujino, T., and Funaki, I., "A Theoretical Analysis for Electrodeless Lissajous Acceleration of HELICON Plasmas," *42nd AIAA Plasmadynamics and Lasers Conference in Conjunction with the 18th International Conference on MHD Energy Conversion (ICMHD)*, AIAA Paper 2011-4008, June 2011. doi:10.2514/6.2011-4008

[15] Emsellem, G., "Electrodeless Plasma Thruster Design," *41st AIAA/ASME/SAE/ASEE Joint Propulsion Conference*, AIAA Paper 2005-3855, July 2005. doi:10.2514/6.2005-3855

[16] Jorns, B., and Choueiri, E., "Thruster Concept for Transverse Acceleration by the Beating Electrostatic Wave Ponderomotive Force," *32nd International Electric Propulsion Conference*, IEPC Paper IEPC-2011-214, Wiesbaden, Germany, Sept. 2011.

[17] Jorns, B., and Choueiri, E. Y., "Experiment for Plasma Energization with Beating Electrostatic Waves," *31st International Electric Propulsion Conference*, IEPC Paper IEPC-2009-199, Sept. 2009.

[18] Jaeger, E., Berry, L., and Batchelor, D., "Full-Wave Calculation of Sheared Poloidal Flow Driven by High-Harmonic Ion Bernstein Waves in Tokamak Plasmas," *Physics of Plasmas*, Vol. 7, No. 8, 2000, pp. 3319–3329. doi:10.1063/1.874197

[19] Myra, J., and D'Ippolito, D., "Toroidal Formulation of Nonlinear-RF-Driven Flows," *Physics of Plasmas*, Vol. 9, No. 9, 2002, pp. 3867–3873. doi:10.1063/1.1496762

[20] Fisch, N., "Theory of Current Drive in Plasmas," *Review of Modern Physics*, Vol. 59, No. 1, 1987, pp. 175–234. doi:10.1103/RevModPhys.59.175

[21] Fisch, N., Rax, J., and Dodin, I., "Current Drive in a Ponderomotive Potential with Sign Reversal," *Physics Review Letters*, Vol. 91, No. 20, 2003, Paper 205004. doi:10.1103/PhysRevLett.91.205004

[22] Maecker, H., "Plasma Jets in Arcs in a Process of Self-Induced Magnetic Compression," *Zeitschrift fur Physik*, Vol. 141, Nos. 1–2, 1955, pp. 198–216. doi:10.1007/BF01327300

[23] Jahn, R., *Physics of Electric Propulsion*, McGraw–Hill, New York, 1968, pp. 240–246.

[24] Choueiri, E. Y., "The Scaling of Thrust in Self-Field Magneto-plasmadynamic Thrusters," *Journal of Propulsion and Power*, Vol. 14, No. 5, 1998, pp. 744–753. doi:10.2514/2.5337

[25] Dodd, C., and Deeds, W., "Analytical Solutions to the Eddy-Current Probe-Coil Problems," *Journal of Applied Physics*, Vol. 39, No. 6, 1968, pp. 2829–2838. doi:10.1063/1.1656680

[26] Skiff, F., Ono, M., and Wong, K., "Excitation of ion Bernstein Waves from Loop Antennas," *Physics of Fluids*, Vol. 31, No. 7, 1988, p. 2030. doi:10.1063/1.866652

[27] Purcell, E., *Electricity and Magnetism*, McGraw–Hill, New York, 1985, pp. 231–234.

J. Blandino
Associate Editor